AIAA JOURNAL
Vol. 41, No. 6, June 2003

Computational Modeling of Damage Growth in Composite Laminates

Shiladitya Basu* and Anthony M. Waas†
University of Michigan, Ann Arbor, Michigan 48109-2140
and
Damodar R. Ambur‡
NASA Langley Research Center, Hampton, Virginia 23681

A progressive damage growth model is developed for composite laminates under compression. The mechanics of damage initiation and growth in a single lamina is modeled in a two-dimensional plane stress setting, using a system of orthotropic nonlinear elastic relations and a set of internal state variables. The latter are associated with different damage mechanisms that are unique to a fiber-reinforced lamina. A thermodynamically consistent set of equations is developed for the evolution of damage growth. The formulation is numerically implemented using the commercially available finite element package ABAQUS. The present method is applied to analyze the problem of damage growth in a compressively loaded notched laminate. Predictions of the model compared against available experimental observations are promising.

I. Introduction

DEVELOPMENT of computational methodologies for the prediction of progressive damage growth in continuous fiber composite laminates is presently an active area of research. Available predictive methods are based on defining strength-based criteria at the lamina level. Based on critical values for tensile, compressive and shear "strengths," these methods compute predefined damage indices that are expressed in functional form in terms of the current stress state. When any of these indices exceeds a predefined critical value, the material is said to have failed.[1] Beyond initial failure, a consistent and rigorous methodology to account for progressive material deterioration has not been investigated thoroughly. An exception to this is the work by Schapery and Sicking,[2] who carried out lamina-level tests and validated the test results by developing a thermodynamically based progressive damage formation and growth model. In these studies Schapery and Sicking assumed that the fiber-direction response is essentially linear (slight elastic nonlinearity in the fiber direction was accounted for), but damage (microcracking and transverse cracking) formation affected the response in the transverse direction. Consequently, internal state variables that are related to the damage mechanisms in the transverse direction were identified, and evolution laws that specify the growth of damage and hence its influence on the transverse direction response were prescribed. In contrast to the transverse direction, in which damage accumulation results in progressively decreasing but smooth variations in instantaneous tangent moduli, damage accumulation in the fiber direction leads to nonsmooth abrupt changes in the corresponding moduli. These changes must be properly captured if progressive damage growth in composite laminates is to be modeled accurately. In the present paper Schapery's theory (ST) is extended to account for fiber-direction damage (both, in tension and compression) by identifying an additional internal state variable associated with the fiber-direction response. By doing this, we have shown that it is possible to follow the progression of damage beyond first kinking in compressively loaded composite laminates using the extended Schapery theory (EST).

Coupon-level tests in the fiber direction, transverse to the fiber direction and off-axis tests are commonly used to obtain material behavior at the lamina level. These tests supply a complete response (stress–strain) curve (usually nonlinear) with valuable information beyond the proportional limit. The present theory (EST) is based on input that uses only these measured and available test data in conjunction with the laminate stacking sequence and geometry of the problem configuration. Thus, the EST introduced here uses readily available fundamental experimental input leading to a method that can find wide ranging utility, well beyond the example problem addressed herein.

The methodology introduced can also be used to predict damage growth in a general laminate. The laminate is assumed to be built up as a stack of lamina. Each lamina is modeled as a nonlinear elastic, homogenized, orthotropic layer that can undergo damage and is governed by EST. Nonlinear elastic behavior is depicted via three polynomial functions of strain. Two of these functions describe the ratio of secant moduli in the fiber and transeverse directions to their corresponding initial values without damage. The third function describes the behavior of poisson's ratio. Damage is incorporated via three internal state variables (ISV). These ISVs are related to "thermodynamic forces" that will be defined subsequently [see Eq. (8)]. Evolution laws for these ISVs can be cast in a manner that is similar to strain energy release rates, as done, for example, in fracture mechanics. However, in EST the criterion of damage growth is implicitly incorporated into the constitutive equations in contrast to the explicit nature of crack growth criterion in classical fracture mechanics. Thus, in EST the evolution equations are those in which the thermodynamic force [Eq. (8)] is equated to the required or critical force [right-hand side of Eq. (7)].

II. Theoretical Development

A. Nonlinear Constitutive Formulation

Schapery[3] developed nonlinear elastic consitutive relations for an orthotropic lamina using a work potential approach, which accounted for the effect of microdamage. The lamina stress–strain relations are

$$\sigma_{11} = Q_{11} f_1 \epsilon_1 + Q_{12} f_{12} I_2, \qquad \sigma_{22} = Q_{12} f_2 I_1 + Q_{22} f_2 \epsilon_2$$
$$\tau_{12} = Q_{66} \gamma_{12} \tag{1}$$

Received 16 May 2002; revision received 30 December 2002; accepted for publication 5 January 2003.

*Graduate Research Assistant, Composite Structures Laboratory, Department of Aerospace Engineering.
†Professor, Composite Structures Laboratory, Department of Aerospace Engineering. Associate Fellow AIAA.
‡Head, Mechanics and Durability Branch. Associate Fellow AIAA.

where

$$Q_{11} = E_{11}/(1 - \nu_{12}\nu_{21}), \qquad Q_{22} = E_{22}/(1 - \nu_{12}\nu_{21})$$
$$Q_{12} = \nu_{12}Q_{22}, \qquad Q_{66} = G_{12}, \qquad \nu_{21} = \nu_{12}E_{22}/E_{11} \quad (2)$$

The functions f_1, f_2, and f_{12} introduce elastic nonlinearity into the constitutive relations. They are defined as

$$f_1 \equiv \frac{E^0(\epsilon_1)}{E_{11}}, \qquad f_2 \equiv \frac{E^{90}(\epsilon_2)}{E_{22_0}}, \qquad f_{12} \equiv \frac{-1}{\nu_{12}}\frac{\mathrm{d}\epsilon_2}{\mathrm{d}\epsilon_1} \quad (3)$$

Function f_1 expresses the ratio between the fiber direction secant modulus E^0 with its initial value E_{11}. This information is available from a coupon-level tensile or compressive test in the fiber direction upto the point of first failure. First failure is associated with fiber kinking (compression) or fiber fracture (tension). Similarly, function f_2 expresses the same in the transverse direction (E^{90} vs E_{22_0}). Function f_{12} expresses the evolution of Poisson's ratio ν_{12}. This can also be characterized using uniaxial tensile loading in the fiber direction. f_1 and f_{12} are functions of ϵ_1, and f_2 is a function of ϵ_2.

Integrals I_1 and I_2 appearing in Eqs. (1) are defined as

$$I_1 \equiv \int_0^{\epsilon_1} f_{12}\,\mathrm{d}\epsilon_1, \qquad I_2 \equiv \int_0^{\epsilon_2} f_2\,\mathrm{d}\epsilon_2 \quad (4)$$

These definitions satisfy the reciprocity condition

$$\frac{\partial\sigma_1}{\partial\epsilon_2} = \frac{\partial\sigma_2}{\partial\epsilon_1} \quad (5)$$

B. Damage Modeling Through Internal State Variables

In the existing literature on damage mechanics as applied to continuous fiber laminated composite materials, the effect of damage is incorporated through the change in transverse Young's modulus E_{22} and in-plane shear modulus G_{12}. For instance, Sun and Chen[4] proposed a one-parameter plastic potential in conjunction with orthotropic incremental plasticity theory to study the evolution of E_{22} and G_{12} in tension. Schapery and Sicking[2] used ST to study the evolution of E_{22} and G_{12}. These studies were not concerned with the state of the lamina beyond first failure in the fiber direction. Yet, it is recognized[5] that such damage is dominant for compression-loaded composite structures. Lamina-level coupon tests in tension have shown that fiber direction modulus E_{11} and Poisson's ratio ν_{12} can be assumed to be independent of microdamage that influence E_{22} and G_{12}. This situation is also true for compression until the onset of kinking. (The axial compression load reaches a maximum limit load at the point in which a kink band starts to form, for example, as shown in Ref. 6.) During kink band formation and propagation, it is likely that microdamage mechanisms do influence E_{11}, ν_{12}, E_{22}, and G_{12}. When the fiber direction strain exceeds the fiber kinking strain, then it is assumed that the postkinking response assumes that depicted in the compression stress–strain relation of Fig. 1. In tension, fiber fracture occurs, and the resulting response is as indicated in the tension stress–strain relation of Fig. 1.

In Schapery and Sicking[2] internal state variables are used to incorporate inelastic behavior in the material response. Earlier, Schapery[7] introduced a more general thermodynamic framework to study materials those undergo damage. In these developments, the total work done in a mechanical process is composed of the inelastic work W_s and the work of deformation W:

$$W_T = W + W_s \quad (6)$$

The irrecoverable portion of total energy W_s can be determined from the material stress–strain response, as shown in Fig. 2. ISVs are described through S_i. Each S_i is associated with a particular

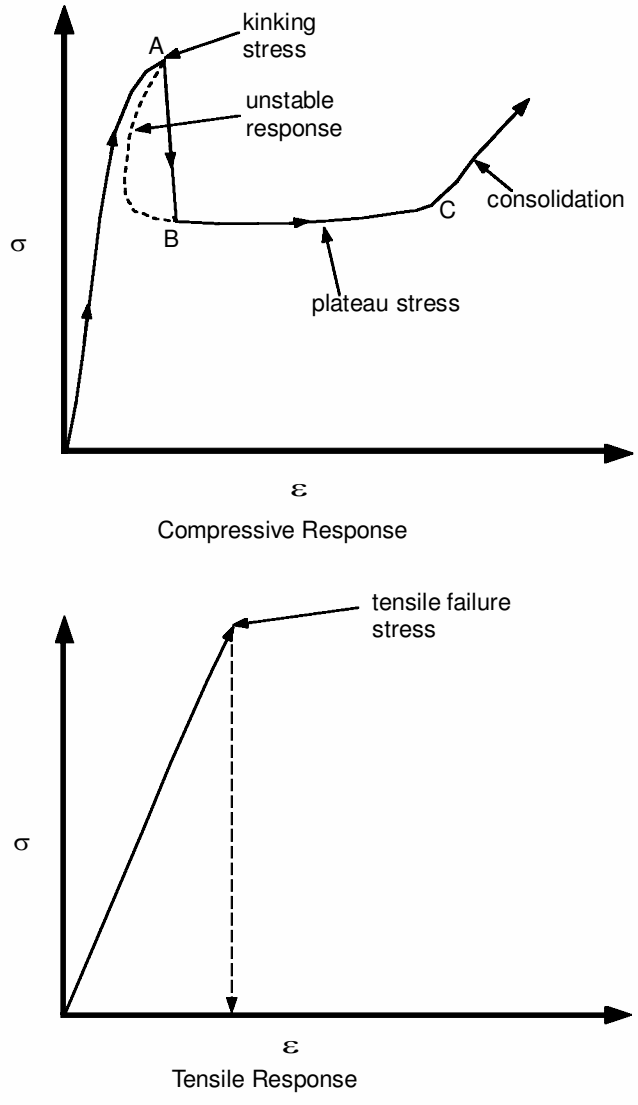

Fig. 1 Typical compressive and tensile stress–strain behavior.

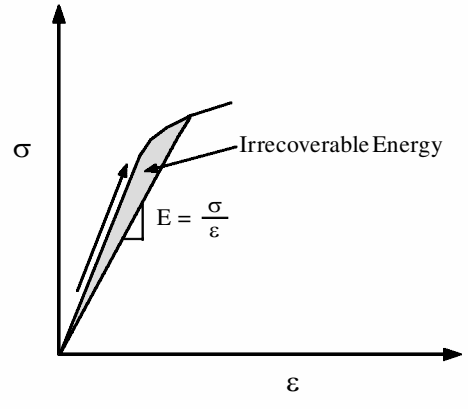

Fig. 2 Determination of irrecoverable energy from stress–strain response.

damage mechanism. To satisfy the path independence of total work, these ISVs have to satisfy the following relation:

$$f_i = \frac{\partial W_s}{\partial S_i} \quad (7)$$

The left-hand side of Eq. (7) is called the thermodynamic force related to the ith ISV. (Note that this f_i has no bearings with the nonlinear elasticity strain functions f_1, f_2, and f_{12}. This is merely the force congujate of every mode of inelasic work.) If the ith driving

force, which is the available thermodynamic force given by Eq. (8), exceeds $\partial W_s/\partial S_i$, then the material undergoes a structural change that is associated with S_i:

$$f_i \equiv -\frac{\partial W}{\partial S_i} \tag{8}$$

Stated another way,

$$\dot{S}_i > 0 \tag{9}$$

However, as pointed out by Schapery,[7] if the available thermodynamic force $(-\partial W/\partial S_i)$ is less than the required thermodynamic force $(\partial W_s/\partial S_i)$, then

$$\dot{S}_i = 0 \tag{10}$$

Furthermore, S_i need not change continuously with the loading.

Schapery considered two ISVs. They were the energies associated with matrix microcracks S and of the transverse intraply cracks S_c, respectively. Inelastic work is described as

$$W_s = S + S_c \tag{11}$$

These ISVs affect the moduli E_{22} and G_{12} through Eq. (12):

$$E_{22} = E_{22_0} e_s(S) e_c(S_c), \qquad G_{12} = G_{12_0} g_s(S) g_c(S_c) \tag{12}$$

Here, E_{22_0} and G_{12_0} are transverse and shear moduli of the virgin material, that is, at zero strain and zero damage; $e_s(S)$ and $g_s(S)$ are functions relating these two moduli to microdamage ISV; and S and $e_c(S_c)$ and $g_c(S_c)$ are functions relating E_{22}, and G_{12} to the transverse cracking ISV S_c. The functions e_s, e_c, g_s, and g_c are expressed as polynomial relations in the respective ISVs.[2] The strain energy density (or work of deformation) can be written as

$$W = Q_{11} I_{11} + Q_{22} I_{22} + \nu_{12} Q_{22} I_1 I_2 + G_{12} \gamma_{12}^2 / 2 \tag{13}$$

where

$$I_{11} \equiv \int_0^{\epsilon_1} \epsilon_1 f_1 \, \mathrm{d}\epsilon_1, \qquad I_{22} \equiv \int_0^{\epsilon_2} \epsilon_2 f_2 \, \mathrm{d}\epsilon_2 \tag{14}$$

To incorporate geometric nonlinearities, Green's strains and the second Piola–Kirchoff stresses need to be used in the expression for W. For small strains Eq. (13) would contain only the first-order terms in the strain-displacement relations. Schapery and Sicking[2] have shown that material nonlinearities as incorporated in Eq. (13) are still significant for fiber-reinforced composites even when inclusion of geometric nonlinearities are not called for (Schapery, R. A., private communication, 2002).

Using Eqs. (7–14), the evolution equation for S and S_c follows as

$$I_{11}\frac{\partial Q_{11}}{\partial S} + (I_{22} + \nu_{12} I_1 I_2)\frac{\partial Q_{22}}{\partial S} + \frac{\gamma_{12}^2}{2}\frac{\partial G_{12}}{\partial S} = -1$$

$$I_{11}\frac{\partial Q_{11}}{\partial S_c} + (I_{22} + \nu_{12} I_1 I_2)\frac{\partial Q_{22}}{\partial S_c} + \frac{\gamma_{12}^2}{2}\frac{\partial G_{12}}{\partial S_c} = -1 \tag{15}$$

In the present work it is assumed that the fiber-direction stiffnesses are unaffected by S and S_c. Thus, the first terms in these equations can be neglected. Also, $\nu_{12}\nu_{21} \ll 1$. Thus, the preceding equations reduce to

$$(I_{22} + \nu_{12} I_1 I_2)\frac{\partial E_{22}}{\partial S} + \frac{\gamma_{12}^2}{2}\frac{\partial G_{12}}{\partial S} = -1$$

$$(I_{22} + \nu_{12} I_1 I_2)\frac{\partial E_{22}}{\partial S_c} + \frac{\gamma_{12}^2}{2}\frac{\partial G_{12}}{\partial S_c} = -1 \tag{16}$$

For an inelastic process the entropy production rate is nonnegative. Hence,

$$\dot{S} + \dot{S}_c \geq 0 \tag{17}$$

The overdots represent temporal derivatives. Physically, $\dot{S}$ and $\dot{S}_c$ are both nonnegative because healing (or reversible damage) is not allowed for in the class of materials considered. Thus the ISVs individually satisfy Eq. (17) as well.

From experiments[2] it has been observed that for small strains S behaves as ϵ^3, based on the fact that moduli are constant for small strains. Thus to express the moduli E_{22} and G_{12} in terms of a polynomial of S, a reduced variable S_r can be used:

$$S_r \equiv S^{\frac{1}{3}} \tag{18}$$

The evolution equation for S_r now becomes

$$(I_{22} + \nu_{12} I_1 I_2)\frac{\partial E_{22}}{\partial S_r} + \frac{\gamma_{12}^2}{2}\frac{\partial G_{12}}{\partial S_r} = -3S_r^2 \tag{19}$$

The effect of transverse interply cracking is not as easily measurable as the effect of microdamage caused by matrix microcracking. An estimate can be obtained using Eq. (19) to approximate S_r, and then using the following relation:

$$S_c = W_T - W - S \tag{20}$$

In the present study it is assumed that matrix microcracking is the only responsible mechanism for transverse property degradation. A detailed discussion of obtaining S_c is provided in Ref. 2. It is possible to include other softening damage mechanisms such as local fiber-matrix debonding and shear banding through S as has been discussed in Ref. 7.

C. Fiber Direction Damage: Extended Schapery Theory

The theory presented up to now is for a continuous evolution of the strain functions f_1, f_2, and f_{12}. In its present form it is inadequate to incorporate postkinking response (compression) or postfracture response (tension) in the fiber direction. The salient features of the fiber-direction response were schematically shown in Fig. 1.

A new ISV associated with fiber-direction damage is introduced to incorporate response beyond kinking (compression) and fiber fracture (tension). It has been observed in laboratory tests that a material behaves differently for tensile and compressive loading along the fiber direction. Although, local fiber microbuckling/kinking caused by the presence of local imperfections is the main mode of failure in compression,[8–14] tensile failure is caused by fiber fracture, appearing as cracks perpendicular to the loading direction.

The tensile response shows a clear loss of stiffness at failure, and the residual strength vanishes immediately after failure. The compressive response shows the presence of residual strength after failure. The postkinked material behavior can be thought of as the response of a different, transformed material. Rajagopal and Srinivasa[15] have established a general thermodynamic framework to address material microstructure evolution in a finite strain setting, following an earlier exposition that contained similar ideas.[16]

With a new ISV introduced, Eq. (11) becomes

$$W_s = S_w + S + S_c \tag{21}$$

The ISV S_w represents the inelastic behavior in the fiber direction caused by compressive kinking or fiber fracture. Hence, S_w is not present in the initial elastic regime. It can be computed from the material stress–strain curve under compressive loading in the fiber direction as shown in Fig. 3. Once kinking or fiber fracture occurs, S_w takes a finite jump. The finite jump in S_w in compression is termed the it kinking toughness. The kinking toughness is unique to a fiber-reinforced lamina and is a measurable quantity. As will be evident in the discussion section, the magnitude of the kinking toughness influences the compressive load-carrying capacity of the lamina. S_w is related to the fiber-direction secant modulus E_{11} via relations similar to the moduli in other directions. Thus,

$$E_{11} = E_{11_0} h(S_w) \tag{22}$$

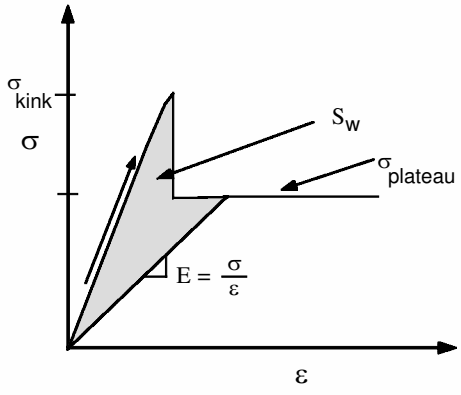

Fig. 3 Determination of S_w from stress–strain response.

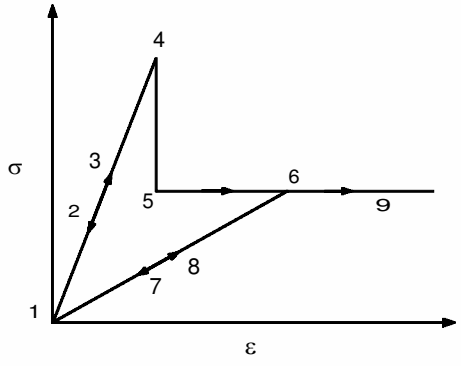

Fig. 4 Loading and unloading behavior of the material.

Using Eqs. (7), (8), and (21), S_w at every state of strain can be obtained as

$$I_{11}\frac{\partial Q_{11}}{\partial S_w} = -1 \tag{23}$$

D. Unloading Characteristics

If the material experiences strain reversal at any point during its loading history, which path it should follow should be properly defined. At the commencement of strain reversal, the material has two options. One option is to trace back the path it followed to reach the present stress–strain state. If this happens, then the work of deformation associated with the strain history would be fully recovered (if unloaded until the zero-stress state). This behavior can be entertained when the material has not undergone any irreversible changes (between origin and point A in Fig. 1).

In the present model it is assumed that the material undergoes irreversible changes in its microstructure and transforms to a "new" material. This implies that the "damaged" material responds as if it were a different material. Among the possible unloading paths (for instance, J2 metal plasticity theories assume that unloading takes place along the initial elastic loading path), we shall assume that unloading occurs along the secant modulus path (Fig. 4). Furthermore, it has been assumed that the material in the kinked zone, whose integrity has been compromised, behaves as a material with degraded properties during unloading and subsequent reloading—essentially, as a new material. The stress–strain relations for the lamina in the postkinked regime are thus given by Eq. (24):

$$\sigma_{11} = Q^*_{11}\epsilon_1 + Q^*_{12}\epsilon_2, \qquad \sigma_{22} = Q^*_{12}\epsilon_1 + Q^*_{22}\epsilon_2$$
$$\tau_{12} = Q_{66}\gamma_{12} \tag{24}$$

where Q^*_{ij} are the plane stress stiffness constants for the new material and defined as follows:

$$Q^*_{11} = E^*_{11}\big/\left(1 - \nu^*_{12}\nu^*_{21}\right), \qquad Q^*_{22} = E_{22}\big/\left(1 - \nu^*_{12}\nu^*_{21}\right)$$
$$Q^*_{12} = \nu^*_{12}Q^*_{22}, \qquad Q_{66} = G_{12}, \qquad E^*_{11} = \sigma_{\text{plateau}}/\epsilon_{11}$$
$$\nu^*_{12} = (\nu_{12}/E_{11})E^*_{11}, \qquad \nu^*_{21} = \nu^*_{12}E_{22}\big/E^*_{11} \tag{25}$$

Here, σ_{plateau} and ϵ_{11} are the plateau stress and instantaneous strain, respectively, along the fiber direction in the postkinked regime. Once strain reversal commences, E^*_{11} becomes the secant modulus at the commencement of strain reversal. A typical loading, unloading, and reloading path is as depicted in Fig. 4.

III. Application of EST

A. Plate with a Hole

The EST introduced in the preceding section was implemented numerically through the commercially available finite element package ABAQUS, and results were obtained for a unidirectional plate with a central circular hole under remote uniform compressive edge displacement loading. The analysis incorporated geometric nonlinearity. Because of symmetry, only a quarter of the plate is analyzed. The problem geometry is shown in Fig. 5. The plate was remotely loaded until the damage zone initiating at the edge of the hole (point J in Fig. 5) reached the boundary of the plate (point K in Fig. 5), simulating a test program in which the plate is loaded to complete failure.

B. Modeling in ABAQUS

1. Geometry

The geometry depicted in Fig. 5 was meshed using plane-stress two-dimensional continuum elements CPS4. To study the effect of higher-order interpolation, one mesh that used CPS8 plane-stress continuum elements was also studied. Further, a mesh that used CPS3 triangular elements was also investigated. End loading was provided by specifying edge displacement Δ at the edge of the plate. During the loading, this edge is free to deform in the y direction. Symmetric boundary conditions were enforced on the two sides adjacent to the hole (sides JK and MN in Fig. 5).

2. Material Model

In the commercially available finit element code ABAQUS, it is possible to introduce user-defined material behavior through user written subroutines. To that end, the user needs to provide the incremental stress–strain relationships or the material Jacobian J and update the stress and/or any internal state variables to their values at the end of each increment. This user subroutine would be called by the ABAQUS solver at every material point, where the user-defined material is included.

The material data for the present study were obtained from Dávila et al.[5] (Table 1). The material is modeled as a homogenized orthotropic nonlinear elastic material obeying EST. With a view to

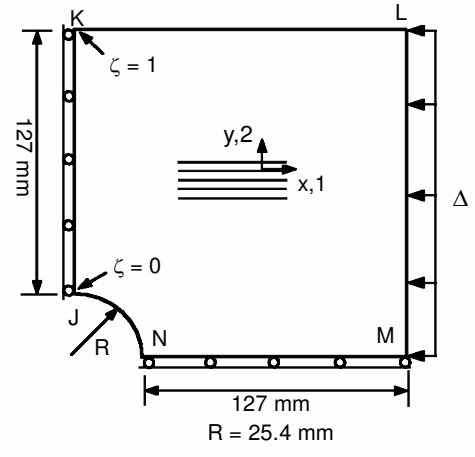

Fig. 5 Geometry of the plate with a hole. (Fiber direction is parallel to the x direction.) A plate thickness of 13.6 mm was used throughout this study.

extending the present work to model stringer-stiffenednotched panels in compression,[5] we were interested in obtaining the complete material response curves for AS4/3501-6. Hence the experimental data given in Schapery and Sicking[2] for AS4/3502 were used to approximate the relevant functional parameters f_1, f_2, f_{12}, $e_s(S_r)$, and $g_s(S_r)$ for AS4/3501-6. Available parameters for AS4/3502 were scaled down by the ratio of moduli of AS4/3501-6 and AS4/3502. A typical coefficient A_{ij} was modified as

$$A_{ij}^{3501} = A_{ij}^{3502}(E^{3501}/E^{3502}) \tag{26}$$

Here E represents the appropriate elastic modulus for the corresponding A_{ij}. The set of parameters corresponding to the AS4/3501-6, 0-deg lamina are given in Table 2.

As stated earlier, in the present work only S_w and S_r are used as damage parameters because the mechanisms of damage that are considered are matrix microcracking and fiber-direction damage.

3. Elements and Meshes Studied

Three meshes were generated using first-order elements. Two of these were with CPS4 elements and one mesh with CPS3 elements. One mesh was also generated with second-order elements CPS8. These meshes are shown in Fig. 6 (and pertinent data about the meshes are presented in Table 3). To check the merit of each of these meshes, a linear analysis with isotropic material properties was performed. Stress $\sigma_{\theta\theta}$ was computed at the integration point closest to the top of the hole (where the largest stress concentration occurs) using the classical result of a plate with a hole in a uniform tensile field and compared against the finite element result. Errors in stress values for each of these meshes are tabulated in Table 4. Further, the stress decay away from the hole was also checked in order to ensure that the meshes adequately captured the stress gradients present in the problem. The present problem is one where internal material instabilities, modeled through the evolution of S_w, are present. Consequently, an arc-length method (the modified Riks method[17] that is available in ABAQUS was used to verify that results obtained through a standard nonlinear solution procedure adequately captured the essence of the load-end shortening response.

Table 1 Material constants

Modulus	AS4/3501-6
E_L, GPa	46.73
E_T, GPa	4.89
G_{LT}, GPa	2.45
ν_{12}	0.34

Table 2 Coefficients used in numerical modeling

Exponent	f_1	f_2(comp)	f_2(tens)	f_{12}
0	1	1	1	1
1	4.429	5.5220	−5.5220	−14.6
2	−29.5346	−43.145	−27.9337	−594.8290

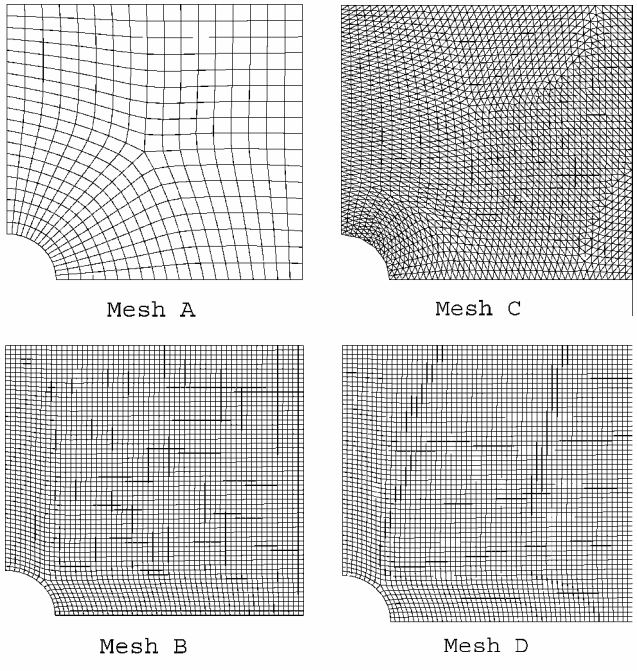

Fig. 6 Meshes used in the analysis (mesh A, CPS4; mesh B, CPS4; mesh C, CPS3; and mesh D, CPS8).

Table 3 Summary of element and nodal data of the meshes used

Mesh parameter	Mesh A	Mesh B	Mesh C	Mesh D
Element type	CPS4	CPS4	CPS3	CPS8
Number of elements	401	3,316	3,565	3,316
Number of nodes	447	3,434	1,877	10,183
Number of degrees of freedom	894	6,868	3,754	20,366

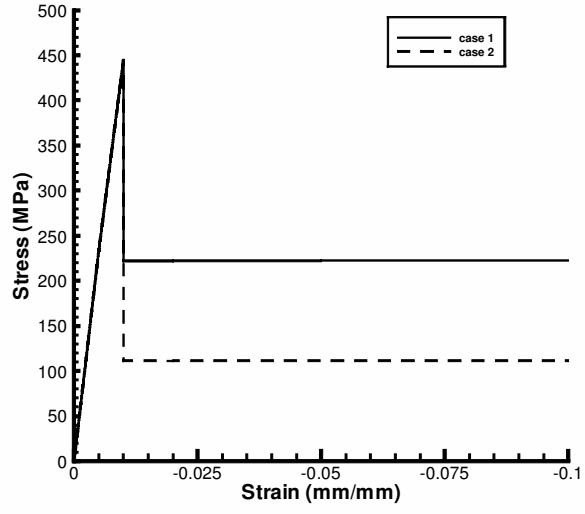

Fig. 7 Idealized fiber-direction stress–strain curve input to ABAQUS.

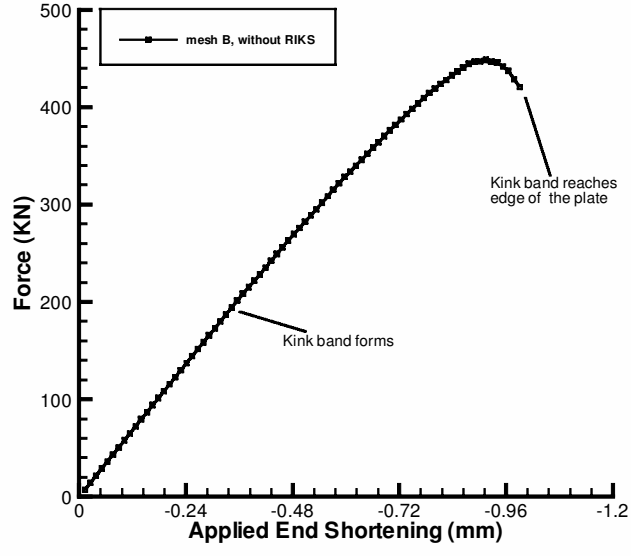

Fig. 8 Global reaction force against end shortening for mesh B using case 1.

IV. Results and Discussion

As indicated by the tabulated results in Table 4, it was deemed that all of the meshes used in this study adequately captured

Table 4 Comparison of different meshes used in the analyses

Mesh	Location of r	Integration point θ, deg	Resultant reaction force on vertical edge JK, KN	σ_{computed}, MPa	$\sigma_{\text{FE result}}$, MPa	Error, %
A	1.049	88.80	222.90	289.51	303.30	4.76
B	1.017	88.93	222.63	309.92	319.30	3.03
C	1.055	88.10	223.08	286.34	274.48	4.14
D	1.009	89.43	222.59	315.71	321.64	1.88

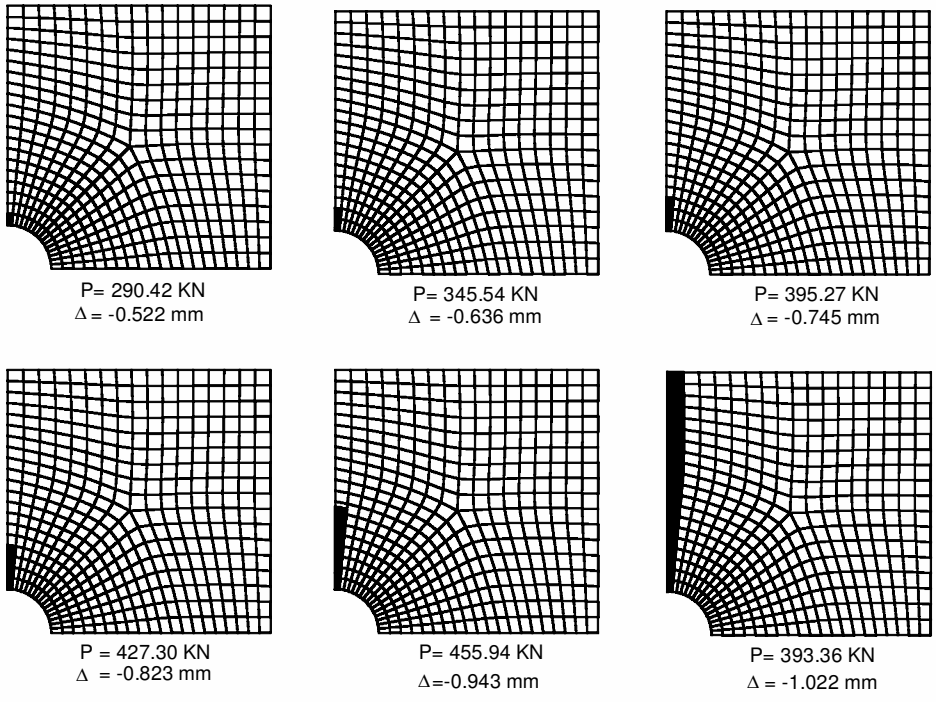

Fig. 9 Initiation and progression of kink band with end displacement at different end shortening for case 1 using mesh A.

the stress magnitudes and stress gradients in the vicinity of the hole.

Mesh A and mesh B with different mesh densities were used to generate the bulk of the finite element results. From the results the variation of resultant reaction force on edge JK, P against the applied end shortening Δ, was obtained. A plot of the fraction of undamaged material remaining in the system against Δ was also constructed. Figures are provided to show the growth of damage through different loading positions for these two meshes. Mesh C and mesh D were used to generate data to analyze the effect of different element types.

The effect of the plateau stress magnitude of the fiber-direction material response on the residual strength carrying capacity of the plate was also studied. This was done by lowering the plateau stress to 25% of the kinking stress (case 2). In case 1 the plateau stress was 50% of the kinking stress (see Fig. 7). Mesh C and mesh D were studied under case 1 only. The results obtained from mesh A and mesh B are discussed first. Results from mesh C and mesh D are discussed later.

Initially, the response of the plate is linear elastic. Therefore the reaction force against the applied end-shortening ($P-\Delta$) curve is a straight line, as shown in Fig. 8. (Slight elastic nonlinearity is incorporated through the f_{ij}; however, this does not show a visible effect on the $P-\Delta$ curve.) When the material elements adjacent to the hole reach a critical strain corresponding to fiber kinking, a damage zone is found to initiate at the edge of the hole. This is depicted in Figs. 9 and 10, where the progression of damage is shown as darkened elements on the finite element grid. (This is shown only for mesh A and mesh B. The salient features of the damage progression in other meshes are also similar.) Beyond kinking, the $P-\Delta$ curve shows a gradual change in slope with kink band propagation as shown in Fig. 11. On the $P-\Delta$ curve the extent of kink growth is indicated as a fractional distance (ζ) from the edge of the hole. (Thus, when this distance $\zeta = 1.0$, the kink band has reached point K at the edge of the plate). When $\zeta \approx 0.4$, the $P-\Delta$ curve goes through a maximum, and beyond this the kink propagation occurs with decreasing remote load.

$P-\Delta$ curves for all of the first-order element meshes (Fig. 6) are plotted for case 1 in Fig. 11. As can be observed, using different element types of the same interpolation order has minimal effect on the $P-\Delta$ curves. Although the mesh densities are quite different between mesh A and mesh B, salient features of the response match quite well. Mesh C results are slightly different than that of mesh A and mesh B, but within the limits of numerical accuracy. All of these elements use linear interpolation in their formulation and thus do not require extensive computer resources. In addition, within the context of the present formulation they can be successfully used to capture deformation localization in a macroscopic setting as has been described here. Notice that the use of the Riks method facilitates capturing the effect of kinking on the global instability of the plate. That is, as shown in Fig. 11, use of the RIKS method results in a $P-\Delta$ response that shows a negative slope beyond the maximum load. The interpretation of this in the context of an experiment is that the far field load drops from the maximum to the final steady value (the last point on the plot) instantaneously. A $P-\Delta$ curve that goes through a load maximum and shows snap-back occurs in a wide variety of structural mechanics problems. A thorough discussion of this type of snap-back in the context of micromechanical analyses of fiber microbuckling and kinking is given in Refs. 10 and 13.

In Figs. 12 and 13 the volume fraction of the undamaged material (damage associated with S_w only) is plotted against Δ for

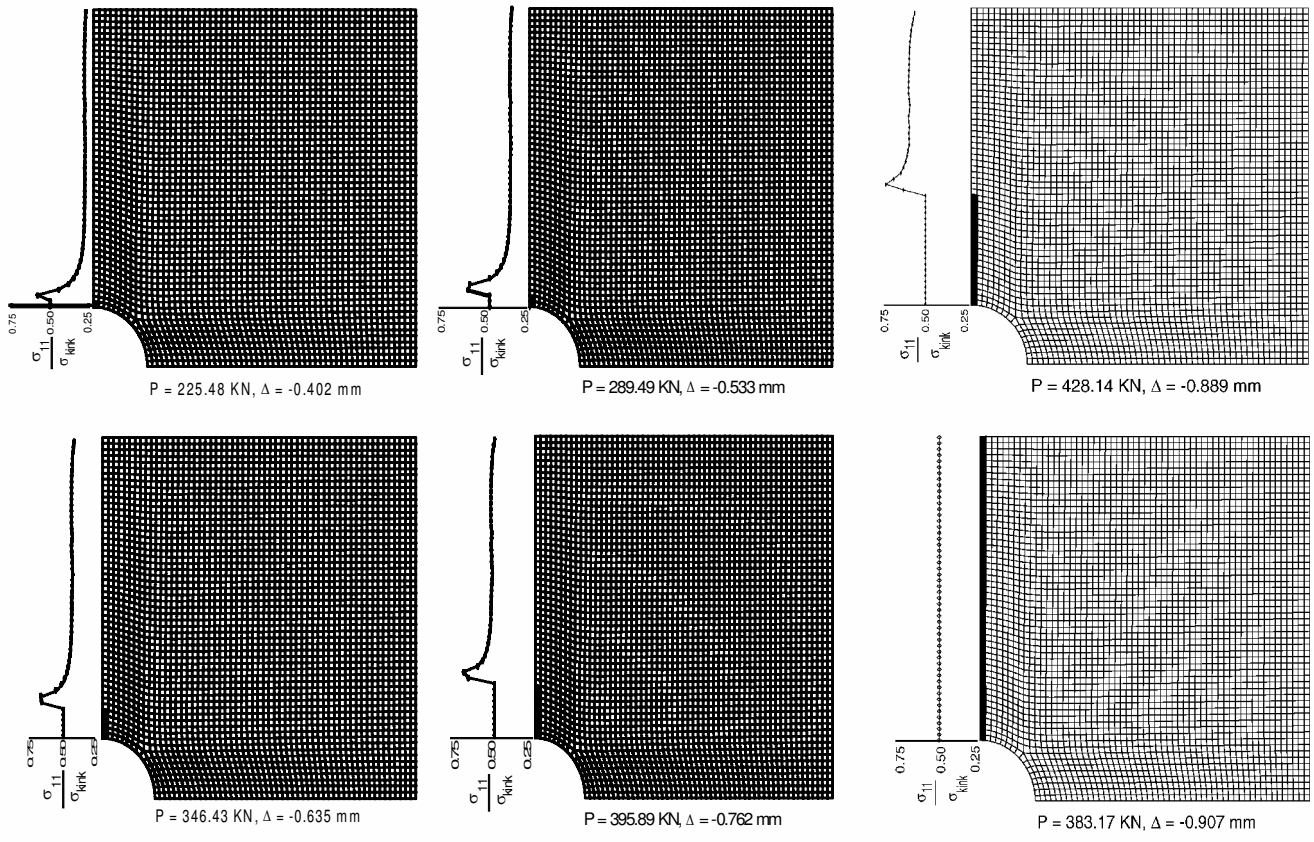

Fig. 10 Initiation and progression of kink band with end displacement at different end shortening for case 1 using mesh B. Accompanying plots show the normalized σ_{11} variation along the side JK.

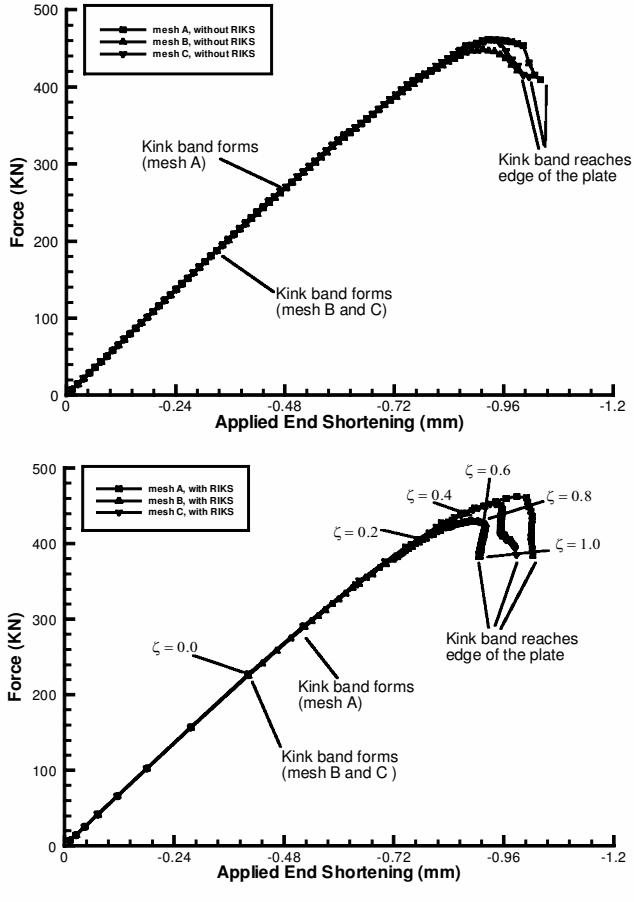

Fig. 11 Global reaction force against end shortening for first-order element meshes. The position of the kink band front, measured as a fractional distance from the hole edge ζ, is indicated on the plots for mesh B.

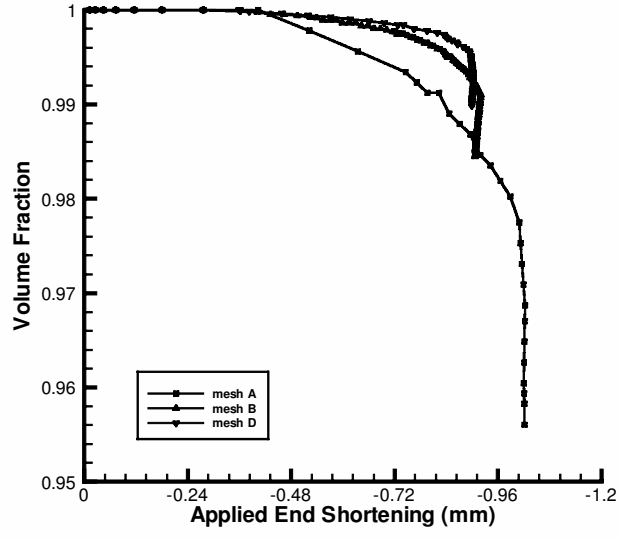

Fig. 12 Lowering of undamaged volume fraction with end displacement for mesh A, mesh B, and mesh D using case 1.

different meshes and different cases. As is evident, as damage progresses, the rate at which the kink band engulfs more and more material increases. The present numerical results are remarkably in good agreement with previous experimental observations[18] on uniply model composite plates with a circular hole, where it was observed that fiber kink banding initiated and propagated in the manner that has been simulated in the present work.

An important aspect of the problem studied is an investigation of the effect of the magnitude of the plateau stress (this magnitude being dictated by the kinking toughness) on the initiation and propagation of damage. To study this effect, two cases as noted earlier are considered. In Fig. 14 the $P-\Delta$ curves corresponding to case 1 and case 2 are shown using mesh B. Notice that the lowering of

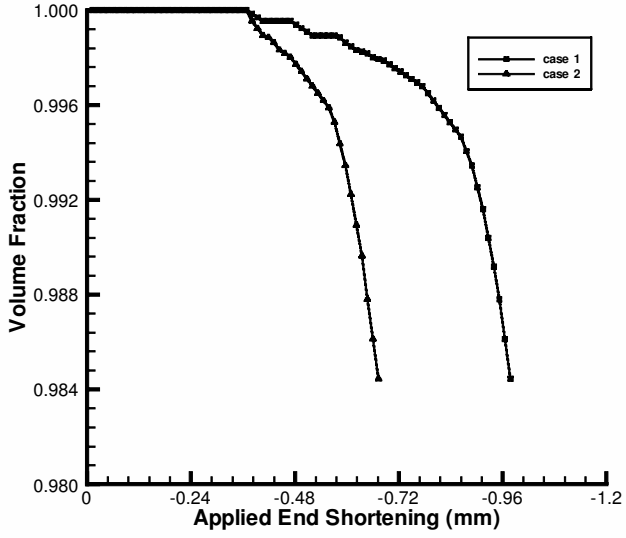

Fig. 13 Lowering of undamaged volume fraction with end displacement for mesh B using case 1 and case 2.

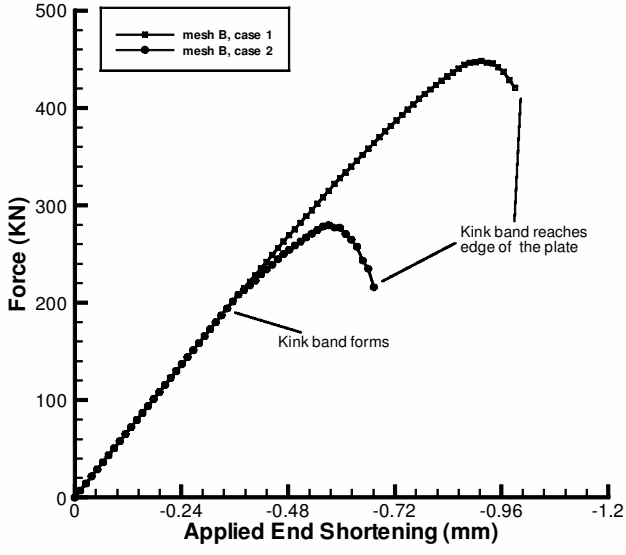

Fig. 14 Global reaction force against end shortening for mesh B using case 1 and case 2.

the plateau stress leads to a drastic reduction (almost 50%) in the maximum load-carrying capability of the notched panel. Thus, both the kinking stress and the plateau stress of the fiber-direction material response are important material characteristics associated with the residual compressive strength of a fiber-reinforced lamina. In fact, as discussed earlier, the area under the fiber-direction compressive stress–strain curve up to the point of the initiation of the plateau stress is termed the kinking toughness, and this parameter is an experimentally measurable quantity. Alternatively, as shown recently,[10,13] micromechanics modeling can be used to extract the kinking toughness from the fiber and matrix nonlinear properties and the fiber volume fraction. In Ref. 10 the authors were able to predict global macroscopic loads on a laminate corresponding to failure initiation at the edge of the hole via the use of micromechanics modeling in conjunction with a local–global finite element methodology. In contrast, Soutis et al.,[19] who model the kink band as a crack, have incorporated the fracture toughness into a cohesive zone model to study failure initiating at the edge of notches.

In the present work the fiber-direction response has been modeled in accordance with micromechanics-based results on kinking reported in Refs. 6, 10, 12, and 13. In Ref. 13 an extensive parametric study has shown how details of the macroscopic fiber direction P response is affected by the size of the micromechanics model, the initial fiber waviness, and details of the matrix material nonlinear response. For instance, the $P-\Delta$ response of the micromechanics model can show snap-back immediately beyond the peak load, and this snap-back or lack of snap-back is related to the size of the kink band region in relation to the size of the overall model. Regardless, the maximum limit load and the plateau load appear to be largely unaffected for fiber misalignments of 1–2 deg. Thus, the assumed macroscopic fiber-direction compression response shown in Fig. 7 has incorporated the essential features of the micromechanics studies.

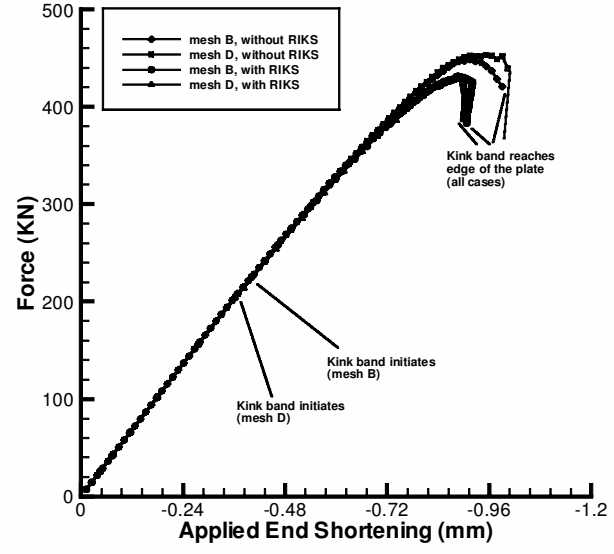

Fig. 15 Global reaction force against end shortening for mesh B and mesh D (with and without modified RIKS method).

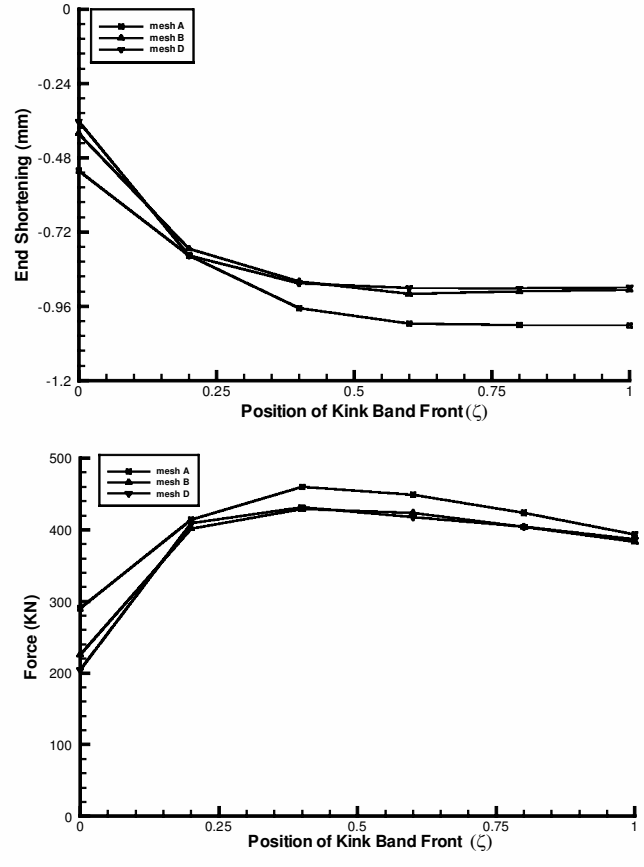

Fig. 16 Global reaction force and end shortening responses with the progression of the kink band (meshes A, B, and D).

Table 5 Summary of results

Analysis type	Mesh A	Mesh B	Mesh C	Mesh D
Data without using RIKS method				
Maximum load, KN	460.84	448.38	462.17	453.27
Displacement, mm	−0.940	−0.914	−0.927	−0.953
Load when kink band reaches K, KN	408.88	420.62	413.11	439.40
Displacement, mm	−1.041	−0.991	−1.016	−1.003
Data using RIKS method				
Maximum load, KN	462.62	430.19	452.83	431.52
Displacement, mm	−0.989	−0.888	−0.931	−0.909
Load when kink band reaches K, KN	384.64	383.17	385.22	386.73
Displacement, mm	−1.024	−0.907	−0.988	−0.899

Results obtained with mesh D (CPS8 elements) are compared against results for mesh B in Fig. 15, whereas the position of the kink band front is plotted against the remote load and end shortening in Fig. 16 for mesh A, mesh B, and mesh D. The results in Fig. 16 show that the kink band growth characteristics are not dependent on the type of mesh used. Furthermore, the results indicate that the kink band growth is unstable beyond a distance, $\zeta \approx 0.4$. As indicated in Fig. 16, when the kink band has traversed to the edge of the plate, the load approaches a value of ≈ 384 kN. This value is consistent with the fiber direction stress–strain response, where it is seen that the plateau stress is 222.5 MPa. Because the elements along edge JK are at this plateau stress, the resultant load on edge JK in the x direction is the plateau stress (σ_{plateau}) multiplied by the section area (13.6×127 mm^2), which turns out to be ≈ 384 kN. A summary of the important features of all of the results are tabulated in Table 5.

V. Conclusions

A nonlinear elastic/inelastic damage methodology has been presented and numerically implemented to study progressive failure in fiber-reinforced composite materials. The methodology is based on an extended version of Schapery theory (EST). EST is based on a thermodynamically consistent internal state variable formulation. The usefulness of EST has been demonstrated by examining the compressive response of a unidirectional notched composite plate. The numerical results capture the experimental observations that have been reported before in the open literature. The present work has addressed the important problem of modeling unstable local material response (fiber kinking) in a global setting, where the structure can still be stable. That is, a macroscopic methodology to analyze compressively loaded composite structures in the presence of locally unstable material response has been provided. The usefulness of knowing the compressive kinking toughness of a fiber-reinforced lamina (measured experimentally or modeled and extracted using micromechanics) has been demonstrated, and its influence on the ultimate load-carrying capability of a structure has been studied via an examination of the change in fiber-direction material plateau stress values. These analyses also showed the effect of different element types and mesh sizes on the numerical response, which is minimal beyond a characteristic element size. The utility of the present work to model laminated composites is far reaching for the analysis and design of damage-tolerant composite structures.

Acknowledgment

The authors are grateful for financial sponsorship through NASA Langley Research Grant NCC-1-01050.

References

[1]Chang, F.-K., and Chang, K. Y., "A Progressive Damage Model for Laminated Composites Containing Stress Concentrations," *Journal of Composite Materials*, Vol. 21, Sept. 1987, pp. 834–855.

[2]Schapery, R. A., and Sicking, D. L., "On Nonlinear Constitutive Equations for Elastic and Viscoelastic Composites with Growing Damage," *Mechanical Behavior of Materials*, Vol. 47, June 1995, pp. 45–76.

[3]Schapery, R. A., "Mechanical Characterization and Analysis of Inelastic Composite Laminates with Growing Damage," *Mechanics of Composite Materials and Structures*, AMD-100, June 1989, pp. 1–9.

[4]Sun, C. T., and Chen, J. L., "A Simple Flow Rule for Characterizing Nonlinear Behavior of Fiber Composites," *Journal of Composite Materials*, Vol. 23, Oct. 1989, pp. 1009–1020.

[5]Dávila, C. G., Ambur, D. R., and McGowan, D. M., "Analytical Prediction of Damage Growth in Notched Composite Panels Loaded in Compression," *Journal of Aircraft*, Vol. 37, No. 5, 2000, pp. 898–905.

[6]Lee, S. H., and Waas, A. M., "Compressive Response and Failure of Fiber Reinforced Unidirectional Composites," *International Journal of Fracture*, Vol. 100, Dec. 1999, pp. 275–306.

[7]Schapery, R. A., "A Theory of Mechanical Behavior of Elastic Media with Growing Damage and Other Changes in Structure," *Journal of the Mechanics and Physics of Solids*, Vol. 38, No. 2, 1990, pp. 215–253.

[8]Schultheisz, C. R., and Waas, A. M., "Compressive Failure of Composites 1. Testing and Micromechanical Theories," *Progress in Aerospace Sciences*, Vol. 32, No. 1, 1996, pp. 1–42.

[9]Waas, A. M., and Schultheisz, C. R., "Compressive Failure of Composites 2. Experimental Studies," *Progress in Aerospace Sciences*, Vol. 32, No. 1, 1996, pp. 43–78.

[10]Ahn, J. H., and Waas, A. M., "Prediction of Compressive Failure in Laminated Composites at Room and Elevated Temperature," *AIAA Journal*, Vol. 40, No. 2, 2002, pp. 346–358.

[11]Yerramalli, C. S., and Waas, A. M., "Compressive Splitting Failure of Composites Using Modified Shear Lag Theory," *International Journal of Fracture*, Vol. 115, No. 1, 2002, pp. 1–14.

[12]Budiansky, B., and Fleck, N. A., "Compressive Failure of Fiber Composites." *Journal of Mechanics and Physics of Solids*, 41, No. 1, 1993, pp. 183–211.

[13]Kyriakides, S., Arseculeratne, R., Perry, E. J., and Liechti, K. M., "On the Compressive Failure of Fiber Reinforced Composites," *International Journal of Solids and Structures*, Vol. 32, Nos. 6/7, 1995, pp. 689–738.

[14]Fleck, N. A., "Compressive Failure of Fiber Composites," *Advances in Applied Mechanics*, Vol. 33, 1997, pp. 43–117.

[15]Rajagopal, K. R., and Srinivasa, A. R., "Mechanics of the Inelastic Behavior of Materials. Part II: Inelastic Response," *International Journal of Plasticity*, Vol. 14, Nos. 10–11, 1998, pp. 969–995.

[16]Rajagopal, K., and Wineman, A., "On a Constitutive Theory for Materials Undergoing Microstructural Changes," *Archives of Mechanics*, Vol. 42, July 1990, pp. 53–57.

[17]Riks, E., "The Application of Newton's Method to the Problem of Elastic Stability," *Journal of Applied Mechanics*, Vol. 39, No. 4, 1972, pp. 1060–1065.

[18]Khamseh, A. R., and Waas, A. M., "Failure of Uniply Model Composites Under Compression," *Journal of Engineering Materials and Technology*, Vol. 114, July 1992, pp. 304–310.

[19]Soutis, C., Smith, F. C., and Matthews, F. L., "Predicting the Compressive Engineering Performance of Carbon Fiber-Reinforced Plastics," *Composites Part A*, Vol. 31, No. 6, 2000, pp. 531–536.

S. Saigal
Associate Editor